

<https://doi.org/10.1038/s41612-024-00843-7>

Robust increase in South Asian monsoon rainfall under warming driven by extratropical clouds and ocean

Check for updates

Yong-Jhih Chen¹, Yen-Ting Hwang¹✉ & Jian Lu²

The responses of South Asian Monsoon (SAM) circulation under global warming are known to be highly uncertain, leading to the widespread of SAM rainfall projections among models. Here, we show that the uncertain SAM circulation in Coupled Model Intercomparison Project Phase 6 models consists of two robust components that partly offset each other: a weakening component linked to a global thermodynamic constraint and a northward shift component understood through a regional 2D energetic perspective. We further attribute the robust northward shift of SAM circulation to positive cloud feedback over the Eurasia Continent and heat uptake in the Southern Ocean. A set of climate model simulations supports the finding that SAM rainfall increase is primarily due to the northward shift of circulation driven by extratropical processes. This energetic perspective opens new avenues for predicting monsoon rainfall by connecting circulation changes to radiative forcing, feedbacks, and ocean heat uptake.

The South Asian summer monsoon (SAM) rainfall has important impacts on agriculture and economy¹. Understanding its responses to global warming is critical to future projections; however, a significant spread exists among the projected changes of SAM rainfall in climate models^{2–4}. Moreover, the observational records are largely influenced by aerosol effects and decadal natural variability^{5–11}, making it even harder to constrain the diverging future projections in climate models.

In many previous studies and the most recent report (AR6) of the Intergovernmental Panel on Climate Change (IPCC), the responses of SAM rainfall to global warming are often understood by partitioning into the thermodynamic and dynamic components^{4,12}. It is well-established that the thermodynamic effect (i.e. increased moisture content) robustly contributes to the increases in SAM rainfall^{13–19}, which can be explained by the so-called “wet-get-wetter” mechanism: as the temperature rises, the moisture content in the atmosphere increases following the prediction of Clapeyron–Clausius equation, which strengthens the convergence of moisture flux in the SAM region. On the other hand, the dynamic effect (i.e. changes in circulation) is identified as the main source of uncertainty^{2–4}. Models do not agree with the changes in SAM circulation strength and the projected circulation exhibits complex spatial structure.

A better understanding of the mechanisms driving the changes in SAM rainfall is critical to narrow down the uncertainty in future projections. In a traditional dry paradigm, monsoons are often viewed as continental-scale land-sea breezes driven by land-sea temperature contrast. While the land-

sea contrast perspective offers a possible explanation for the weakening of SAM rainfall associated with the enhanced Indian Ocean warming in the observational record²⁰, it fails to explain the future projections of SAM in climate models, which suggest that the SAM circulation weakens while the land-sea temperature contrast increases under warming^{4,14,21–24}. A more complete paradigm, the recently emerging global energetic perspective, interprets monsoons as moist energetically direct circulations^{25,26}. The monsoon circulations are intrinsically coupled with convection and act to diverge the energy away from their ascending branches; those atmospheric energy transport, in the meantime, must be constrained by global energy budget^{27–29}. This perspective successfully captures the regional precipitation migration over South Asia, including its seasonal variability^{30–32} as well as the responses to external forcing³³. However, how can this energetic perspective improve our understanding of SAM responses under global warming remains to be explored.

Building upon the energetic perspective, we analyze outputs from the Coupled Model Intercomparison Project Phase 6 (CMIP6) archive. The “abrupt-4xCO₂” experiment, as well as a “shared socioeconomic pathway” (ssp370) experiment, are used to illustrate the responses of the climate system in an idealized warming scenario and a more realistic emission scenario, respectively. Our analysis shows that the long-standing inter-model spread of SAM circulation’s projection represents the combination of the two robust components. The first is a weakening component, aligning with the global mean radiative constraint¹⁵. The second, a northward shift of

¹Department of Atmospheric Sciences, National Taiwan University, Taipei City, Taiwan. ²Atmospheric, Climate, and Earth Sciences Division, Pacific Northwest National Laboratory, Richland, USA. ✉e-mail: ythwang@ntu.edu.tw

deep convections, can be understood through a 2D energetic perspective³⁴, and is attributable to Southern Ocean heat uptake and positive cloud feedback over Eurasia. The two components exhibit remarkable agreement among models and offer pathways to narrow down the uncertainty in future projection.

Results

Excess SAM rainfall driven by the shift of circulation

We start our analysis by reproducing the large inter-model spread in monsoon circulation and its contribution to precipitation uncertainty via performing the traditional moisture budget analysis introduced in previous literature^{4,12} (Method) (Fig. 1a, b). Despite that all climate models predict an

increase in monsoon rainfall in response to anthropogenic forcing (Fig. 1a), a significant spread exists in magnitudes (0.1–1.9 mm/day); even for an idealized forcing of quadrupled CO₂, the magnitudes can vary from 0.4 to 1.8 mm/day. Models do not agree on the sign of the contribution from circulation changes (the QdV term in Fig. 1b); additionally, the circulation changes are highly uncertain within the SAM monsoon region (see the lack of dots in Fig. 1d), challenging our confidence in predicting regional rainfall changes.

A deeper understanding of the circulation changes may be achieved by identifying its root causes. Here, we detangle the uncertain circulation changes by isolating the “weakening component” (Fig. 1e), which represents the slowdown of climatological circulation and is well-understood via the

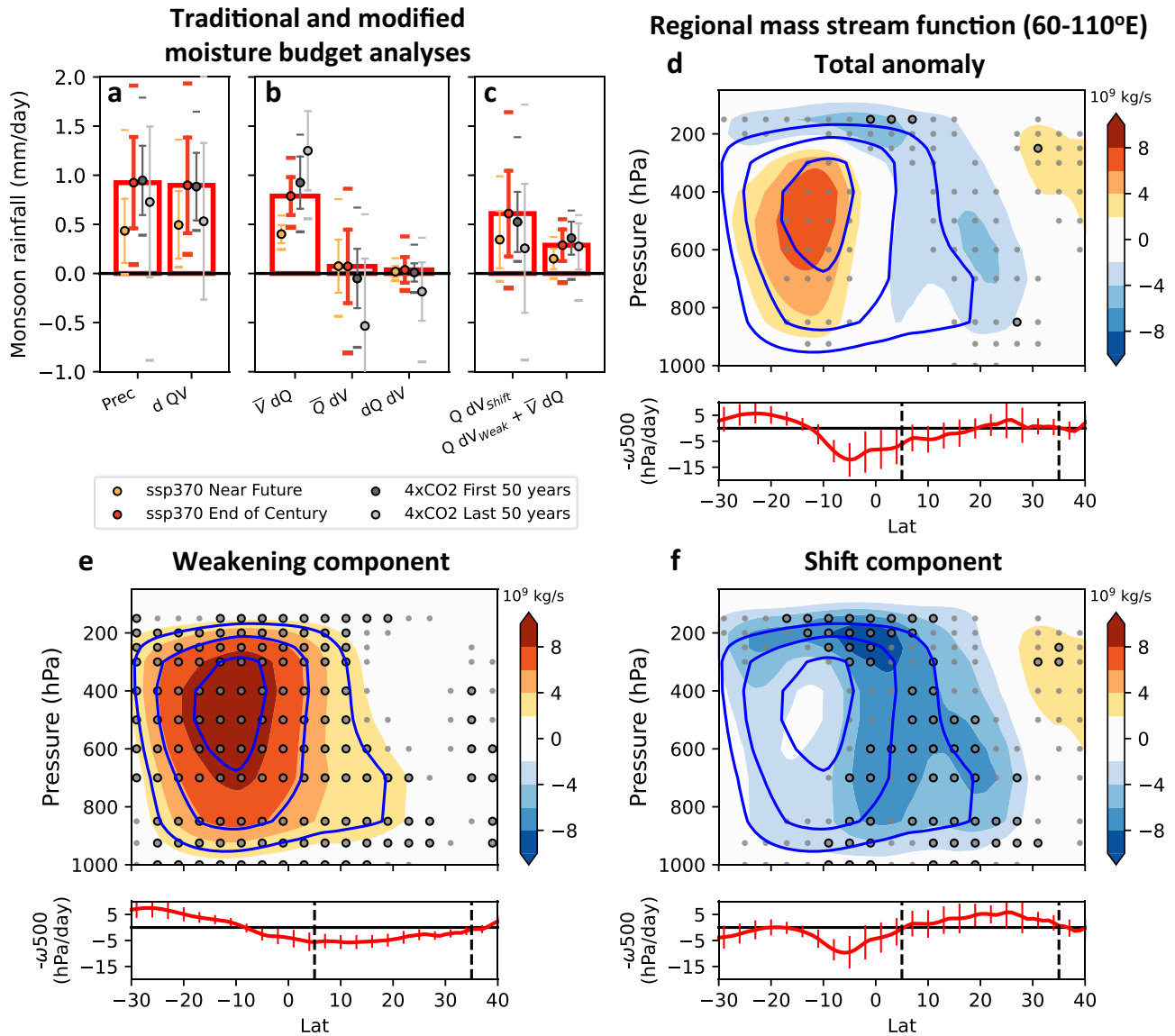


Fig. 1 | Changes in sectoral zonal mean circulation and their contributions to rainfall increase in SAM region under global warming. a–c JJA-mean changes of monsoon rainfall (60–100° E, 5–35° N) and moisture budget decomposition in the ssp370 and abrupt-4xCO₂ simulations. For the ssp370 simulation, the anomalies are relative to the climatology of years 1981–2000 of the Historical simulation; the average in the near future (2041–2060) and the end of century (2081–2100) are shown. For the abrupt-4xCO₂ simulation, the anomalies are relative to the piControl climatology; the average in the first 50 years and last 50 years (101–150) are shown. The dots show the multi-model mean values; the error bars and the horizontal lines indicate the range of one inter-model standard deviation and the maximum/minimum values, respectively. The multi-model mean anomalies by the end of century in

ssp370 simulation are emphasized in red bars. d–f JJA-mean changes in sectoral zonal mean circulation by the end of century in ssp370 simulation. (Upper panel) Regional mass stream function anomaly within 60–110° E. The contours show the base climate with an interval of 20×10^9 kg/s (zero contours omitted); the shadings show the total anomaly (d) and its weakening component (e) and shifting component (f). The small / large dots indicate over 80%/100% of the models agree with the signs. (Lower panel) Multi-model mean of anomalous negative omega at 500hPa, zonally averaged through 60–110° E. The error bars indicate the range of one inter-model standard deviation. The vertical dashed lines mark the SAM region. Positive indicates ascending motion.

global radiative constraint^{15,35}, from the rest of the circulation changes (Fig. 1f) (see Method). This weakening component exhibits a robust descent between roughly 5° S and 30° N, which is confined to the climatological circulation (Fig. 1e). The residual reveals a northward shift of convection zone (Fig. 1f): the anomalous ascent is concentrated over the SAM region, with the peak located at the western coast of Indian Peninsula (Supplementary Figure 1), while the anomalous descent occurs at the equatorial region (Fig. 1f). The “shift component”, representing this northward shift of convection zone, is a robust feature in all models and the pattern is in good agreement with the spatial distribution of multi-model mean precipitation changes (Supplementary Figure 1b–e). The analysis above suggests the notoriously uncertain SAM circulation changes consist of two key components that are remarkably consistent across models (see the dots in Fig. 1e, f). The shift of convective zone toward the SAM region tends to enhance the SAM rainfall, while the weakening of circulation tends to suppress it.

Existing theories suggest a close connection between the weakening of circulation and the thermodynamic responses of the atmosphere^{15,21,35–39}, which is also evident by the high negative correlations between the impacts of circulation weakening and the effects of moistening of the atmosphere on SAM rainfall (−0.69/−0.78 by the end of century in ssp370 simulation and in the first 50 years of abrupt-4xCO₂ simulation, respectively; Supplementary Fig. 2). As required by the atmospheric energy balance in the tropics¹⁵, the rapid increase in moisture content following the C–C equation (~6.5%/K) under global warming must be compensated by a slowdown of overturning circulation, to maintain a moderate increase in convective heating rate (~2%/K) that matches the relatively slower increase in radiative cooling rate. In this context, the weakening of the tropical circulation can be viewed as a compensating factor for the increase in moisture. If we combine the moistening of the atmosphere ($\bar{V}dQ$ in Fig. 1b) and the weakening of circulation ($Q dV_{weak}$) into the “thermally-driven” component ($\bar{V}dQ + Q dV_{weak}$), it is found to account for only a small portion of the projected rainfall increase (Fig. 1c). Instead, the northward shift of circulation ($Q dV_{shift}$ in Fig. 1c) predominately drives the increase of SAM rainfall, and accounts for the majority (88% by the end of the 21st century in ssp370 simulation and 75% in the first 50 years of abrupt-4xCO₂ simulation) of its inter-model variance.

Attribution of the shift of SAM circulation

Given the dominance of the shift component in the model ensemble mean response of the SAM rainfall and the inter-model spread in the SAM projections, it is important to understand the underlying mechanisms that drive the northward shift of the circulation. From the energetic perspective^{27,40}, the shift of tropical precipitation and the associated circulation anomalies (Fig. 1f) are expected to follow the shift of the energy flux equator (EFE, Method), the latitude where the atmospheric energy transport vanishes and diverges meridionally^{34,41}. Indeed, in the ssp370 and abrupt-4xCO₂ simulations, the regional EFE over the SAM longitudinal sector (“regional EFE” hereafter) shows a robust northward shift (Fig. 2a), consistent with the robust shift of precipitation toward the SAM region shown in Fig. 1a and Supplementary Fig. 1. The shift of regional EFE is significantly correlated with the changes in SAM rainfall in most cases, except by the end of century in the ssp370 simulations; it also explains the time-evolving changes of SAM rainfall from the near future toward the end of century in the ssp370 experiment, and the differences between the first and last 50 years in the abrupt-4xCO₂ experiment. These results suggest a close connection between the shift in regional EFE and changes in SAM rainfall, and the processes that drive the former may also be important for the latter.

The shift of regional EFE is a manifestation of the anomalous atmospheric energy transport tied to the global energy budget. When the climate system is perturbed by anthropogenic forcing, the energy sources and sinks of the atmosphere are redistributed, as demonstrated by the anomalous energy flux potential³⁴ (Method) in Fig. 2b.

The positive and negative energy flux potential roughly correspond to the energy sinks and sources of the atmosphere, respectively, and the local energy balance is maintained by the atmospheric energy transport going up the gradient of energy flux potential. The energetic viewpoint interprets the tropical overturning circulation as part of the global energy balance and suggests a teleconnection between tropics and extra-tropics: the anomalous energy flux potential in the tropics largely reflects the extension of the anomalous energy source over the extra-tropical continents in the Northern Hemisphere, as well as the anomalous energy sinks over the North Atlantic and Southern Ocean. Roughly consistent with the anomalous energy flux potential in the tropics, rainfall increases over the regions with anomalous energy sources, including the SAM region and the equatorial western Pacific, and decreases over the regions with anomalous energy sinks, including the Northeast Pacific and the equatorial Indian Ocean. The correspondence between the anomalous energy flux and the pattern of rainfall anomalies is consistent with Mamalakis et al.⁴², which argues that the zonal contrasting shift of ITCZ in the Eastern Pacific–Atlantic sector and Eurasian sectors can be explained by regional atmospheric energy transport and local EFE shift.

Zooming into South Asia, the anomalous energy source to the north and the anomalous energy sink to the south build up an anomalous gradient of energy flux potential, indicating an anomalous southward atmospheric energy transport. As the climatological energy transport of the atmosphere to the north of EFE and reversely to the south of EFE, an anomalously southward energy transport would shift the regional EFE, the latitude with zero meridional atmospheric energy transport, northward. The energy perspective also allows us to mathematically decompose the energy flux potential to the energy sources and sinks in each region (Method⁴³) and perform a quantitative attribution for the northward regional EFE shift. Most of the northward shift of EFE in the South Asian sector can be traced to extra-tropical processes (see Fig. 3a for ssp370 and Supplementary Fig. 3 for abrupt-4xCO₂). In particular, it is mainly driven by the energy source due to the positive cloud feedback over the Eurasia Continent (Fig. 3d and Supplementary Fig. 3d), and the energy sink due to the anomalous ocean heat uptake over the Southern Ocean (Fig. 3c and Supplementary Fig. 3c). Conversely, local energy sources and sinks near the SAM region are highly uncertain and contribute mainly to the inter-model spread.

The diagnoses above reveal the strong spatial dependence of the energetic responses of the climate system (Fig. 3b and Supplementary Fig. 3b). Specifically, cloud feedback and anomalous ocean heat uptake play critical roles in shifting the regional EFE (Fig. 3a) and, consequently, the precipitation patterns of the SAM. The positive cloud feedback in the northern Eurasia Continent is robust across models (dots in Fig. 3d), dominating the TOA flux response (contours in Fig. 3d). The positive cloud feedback over extratropical land has not been extensively discussed in the literature, while one existing study suggests that it is related to the soil moisture deficit over summer land: the robust extra-tropical land drying leads to a rapid decrease in the relative humidity⁴⁴, which, in turn, gives rise to reduced cloud cover and increased insolation (Supplementary Fig. 4). On the other hand, the enhanced heat uptake over the Southern Ocean has been extensively studied and understood as a result of the climatological upwelling in the Southern Ocean, which constantly ventilates the upper ocean with cold water from the deep^{45–48}. In summary, our results suggest the robustness of increases in SAM rainfall arises from the cloud feedback and anomalous ocean heat uptake in the extra-tropics. As the two processes are associated with fundamental physical constraints, they are robust across models and can even be observed in the recent observational records (Supplementary Fig. 5).

Experiments with suppressed cloud or ocean processes

To verify our hypothesis – that the extra-tropical cloud feedback and changes in ocean heat uptake are responsible for most of the northward shift of SAM rainfall – we disable these processes in a fully-coupled model, CESM1, and evaluate their impacts. Several experiments are performed,

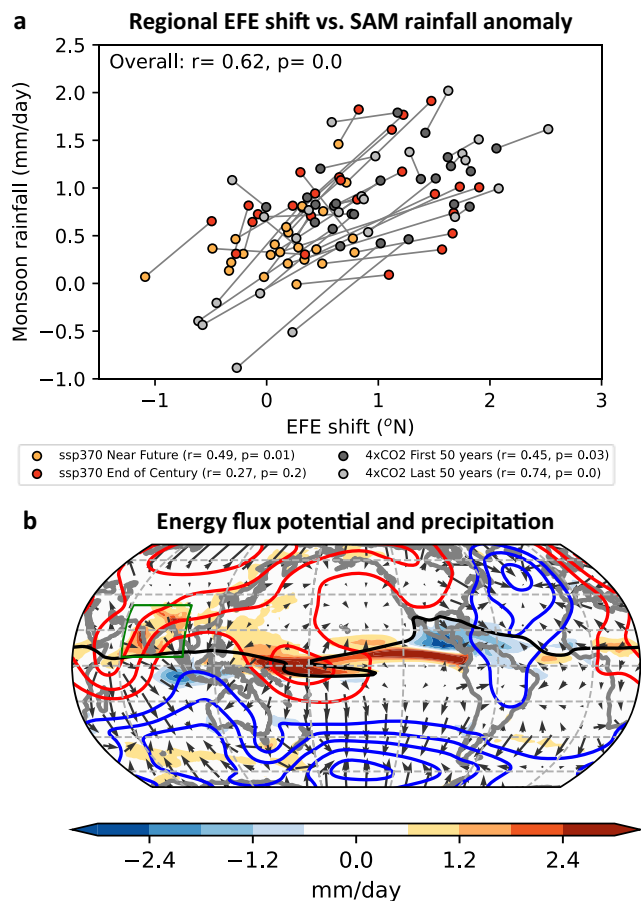


Fig. 2 | Relationship between the changes of energy flux potential and precipitation. **a** CMIP6 JJA-mean monsoon rainfall anomalies versus shifts of regional EFE over 60–100° E. For each model, the former and latter periods of ssp370 and abrupt-4xCO2 simulations are respectively connected with lines. The Pearson correlation coefficient (r) and the p -value of the correlation (p) for each simulation and period are marked in the parentheses in the legend, and the overall correlation and p -value, calculated by all the dots in the figure, are marked at the upper-left corner. **b** Anomalies by the end of century in ssp370 simulations. The shading shows anomalous precipitation and contours show the anomalous energy flux potential (red and blue contours indicate negative and positive values, respectively). The vectors represent the gradient of energy flux potential, i.e. the divergent component of atmospheric energy transport. The thick black lines indicate the energy flux equator (EFE) in the base climate.

including a pre-industrial control simulation (PI), a standard abrupt-4xCO2 simulation (4xCO2), and three partially-coupled abrupt-4xCO2 simulations with suppressed Eurasia Continent cloud feedback (EAcloud_off), or suppressed impacts of Southern Ocean heat uptake (SOHU_off), or with both the processes suppressed (Both_off) (see Method for a more detailed description).

When cloud feedback over Eurasia and Southern Ocean heat uptake are disabled, the increasing rainfall projected in the 4xCO2 simulation vanishes (compare Fig. 4b with a). The summertime rainfall decreases in most of the SAM region except in the southern flank of the Tibetan Plateau. Further analysis (Fig. 4c) shows that the increase in SAM rainfall in the simulation without Eurasian cloud feedback and Southern Ocean heat uptake is reduced by 68% compared to the standard 4xCO2 simulation (Fig. 4c); the reduction is contributed by both the impacts of Eurasia Continent extra-tropical cloud feedback (i.e. 4xCO2 - EAcloud_off) and Southern Ocean heat uptake (i.e. 4xCO2 - SOHU_off) with excellent additivity. Moreover, the moisture budget reveals that the contribution of the shift component disappears when both the Eurasian cloud feedback and the Southern Ocean heat uptake are disabled. These results strongly support the

notion that cloud feedback in the extra-tropics of the Eurasia Continent and the heat uptake over the Southern Ocean play a vital role in the robust increase of SAM rainfall.

Discussion

The large uncertainty in the projection of the regional monsoon change under a warming climate has been a long-standing challenge for the climate change research community. Taking an energetic perspective and aided with purposefully designed feedback denial experiments, we find that the overall SAM precipitation response to the increasing greenhouse gas forcing can be thought of as being driven by the superposition of a weakening and a northward shifting component of the monsoon circulation, both being robust with respect to their own climatology among the CMIP6 models. The energetic analysis suggests that the northward shift of the monsoon circulation and the corresponding precipitation is associated with the strong gradient in the energy flux potential over the SAM region, driven by the positive cloud feedback over the Eurasia Continent and the anomalous heat uptake over the Southern Ocean.

Through the energetic pathway, the shift of the SAM circulation and precipitation are associated with the contrast in energetic feedbacks between the northern land and the Southern Ocean under the forcing of increasing greenhouse gases, as demonstrated by the schematic diagram in Fig. 5. The atmosphere tends to gain energy over the continents and lose energy over the ocean in the extra-tropics (light red and light blue arrows in Fig. 5), leading to the inter-hemisphere energy imbalance which demands adjustments of regional circulation around the SAM region (the vertical cross-section in Fig. 5). This global energetic perspective should be contrasted with the conventional view of the tropical monsoon, which focuses on the local land-sea contrast in temperature and/or thermal inertia. While the rapid warming over lands is a robust feature across models and is also consistent with the northward shift of SAM low-level circulation^{7,24,49–54} and increased SAM rainfall^{7,54}, our partially-coupled simulations reveal that the rainfall is reduced in most regions over South Asia in the **Both_off** simulation (Fig. 4b), even in the presence of increased land-sea temperature contrast (Supplementary Fig. 6).

Our results also offer another perspective on the source of uncertainty underlying the changes in SAM rainfall. The inter-model spread in the SAM rainfall is mainly determined by the shift of circulation (Fig. 1c). The energetic perspective suggests the uncertainty is mainly caused by uncertainty in local cloud feedback and ocean processes in the tropics (Fig. 3a). Regressing the energy fluxes onto the SAM rainfall anomalies suggests the uncertainty is correlated to a zonal dipole of surface flux anomalous in the tropical Indian Ocean, as well as a meridional dipole of cloud feedback over the tropics (Supplementary Fig. 7). As such, while the robust extra-tropical processes are more responsible for the ensemble mean SAM response, the local ocean and cloud radiative feedbacks in the tropics are more responsible for the model uncertainties in the SAM precipitation projections under global warming. Constraint of the local cloud feedback over the SAM region, and the air-sea interaction over the tropical Indian Ocean, may narrow the uncertainty in SAM rainfall. Nevertheless, it should be reminded that the uncertainty in the ssp370 simulations is not solely driven by the responses to the CO2 forcing. The uncertainty caused by other forcings, e.g. the aerosol forcing, may also contribute to the uncertainty of SAM rainfall, leading to the insignificant correlation between SAM rainfall and regional EFE shift by the end of century in the ssp370 simulations; those contributors other than CO2 forcing are, though, beyond the scope of this study.

The global energetic perspective also serves to bridge the long-standing challenge of predicting monsoon circulation response to climate change with the literature on climate sensitivity⁵⁵. Changes in atmospheric energy, including variations in emissions, radiative feedbacks, ocean circulation, and land processes, can all affect monsoon circulation. Moreover, since climate feedbacks and surface turbulent fluxes are inextricably linked to model physics and parameterizations, the energetic perspective could shed light on climate model developments that may help to reduce uncertainties in monsoon projections. This understanding of monsoon circulation shifts

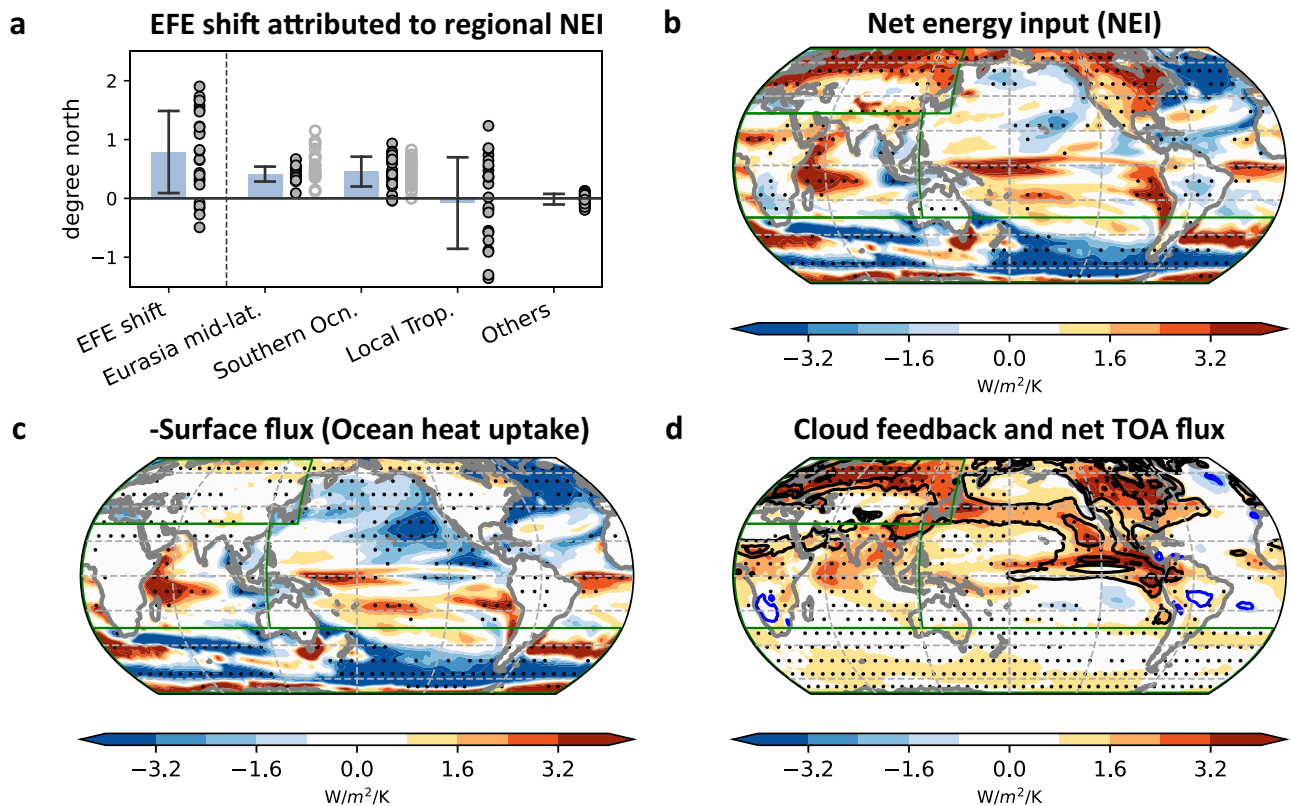


Fig. 3 | Attribution of the shift of regional energy flux equator in JJA. **a** Regional EFE shift by the end of century in CMIP6 ssp370 simulations, and contributions from anomalous NEI of each region (green boxes in **b–d**), estimated by their implied energy transport (see Method). The bars show the model-mean values, the ranges indicate ± 1 standard deviation of inter-model spread, and the black dots represent the values of each model. In the Eurasia mid-latitudes, the gray dots represent the

contribution from cloud feedback alone; in the Southern Ocean, the gray dots represent the contribution from surface flux alone. **b**, **c** Anomalous NEI and surface flux. **d** Cloud feedback (shading) and anomalous TOA flux (contour; black and blue contours indicate positive and negative values, respectively). In (**b–d**), positive values indicate energy into the atmosphere; dots indicate over 80% of the models agree with the signs.

gained here may have direct implications for the response of extreme precipitation over the SAM regions to climate change, which has been linked to the northward migration of synoptic systems from the ocean to land^{22,56}.

Methods

CMIP6 data

To illustrate the responses under anthropogenic forcing, the “shared socioeconomic pathway” simulations under a median-high emission scenario (ssp370) are analyzed; the periods of the near-future (2041–2060) and the end of century (2081–2100) are used, and the anomalies are relative to a baseline climate, defined as the climatology of the years 1981–2000 in the “historical” simulation.

Additionally, the “abrupt-4xCO2” simulation is used to demonstrate the responses under a more idealized scenario of quadrupled CO₂ level. The first 50 years, as well as the period of years 101–150, are used to demonstrate the responses on decadal and centennial timescales. The baseline climate is defined as the climatology in the “piControl” simulation.

For the historical/ssp370 simulations, 25 models that provide all necessary variables are used; for the piControl/abrupt-4xCO2 simulations, a total of 24 models are used (Supplementary Table 1).

Decomposing the shift and weakening components of circulation changes

The changes in circulation are partitioned into the “weakening component” and “shift component” as follows. First, for each model, we define a weakening index α and an error function E :

$$E \equiv \left(\omega_{forced} - \alpha \omega_{base} \right)^2. \tag{1}$$

Where ω_{forced} and ω_{base} represent the total pressure velocity at 500hPa in the forced climate (ssp370 or abrupt-4xCO2 simulations) and baseline climate (historical or piControl simulations), respectively. The weakening index α is chosen to minimize the area-weighted mean of E within the South Asia region (60–110° E, 15° S–35° N), which is generally between 0.7 and 0.95. By doing so, $\alpha \omega_{base}$ describes to what extent the circulations in the baseline climate should be weakened to best match the circulations in the perturbed climate.

Once the weakening index α is determined, the weakening component of circulation anomaly can be defined as the anomaly induced by the overall weakening of circulation:

$$W_{weak} = (\alpha - 1)W_{base}, \tag{2}$$

where W represents wind field (u, v, w). The differences between total anomaly and the weakening component are then defined as the shift component, as it mainly represents the northward shift of deep convections (Fig. 1f):

$$W_{shift} = (W_{forced} - W_{base}) - (\alpha - 1)W_{base} = W_{forced} - \alpha W_{base}. \tag{3}$$

Moisture budget

Following Seager et al.¹², the anomalous precipitation under warming can be written as:

$$dP = dE - \frac{1}{\rho g} \int_0^{ps} [\nabla \cdot (\bar{v}dQ) + \nabla \cdot (\bar{Q}dV) + \nabla \cdot (dVdQ)] dp + residual, \tag{4}$$

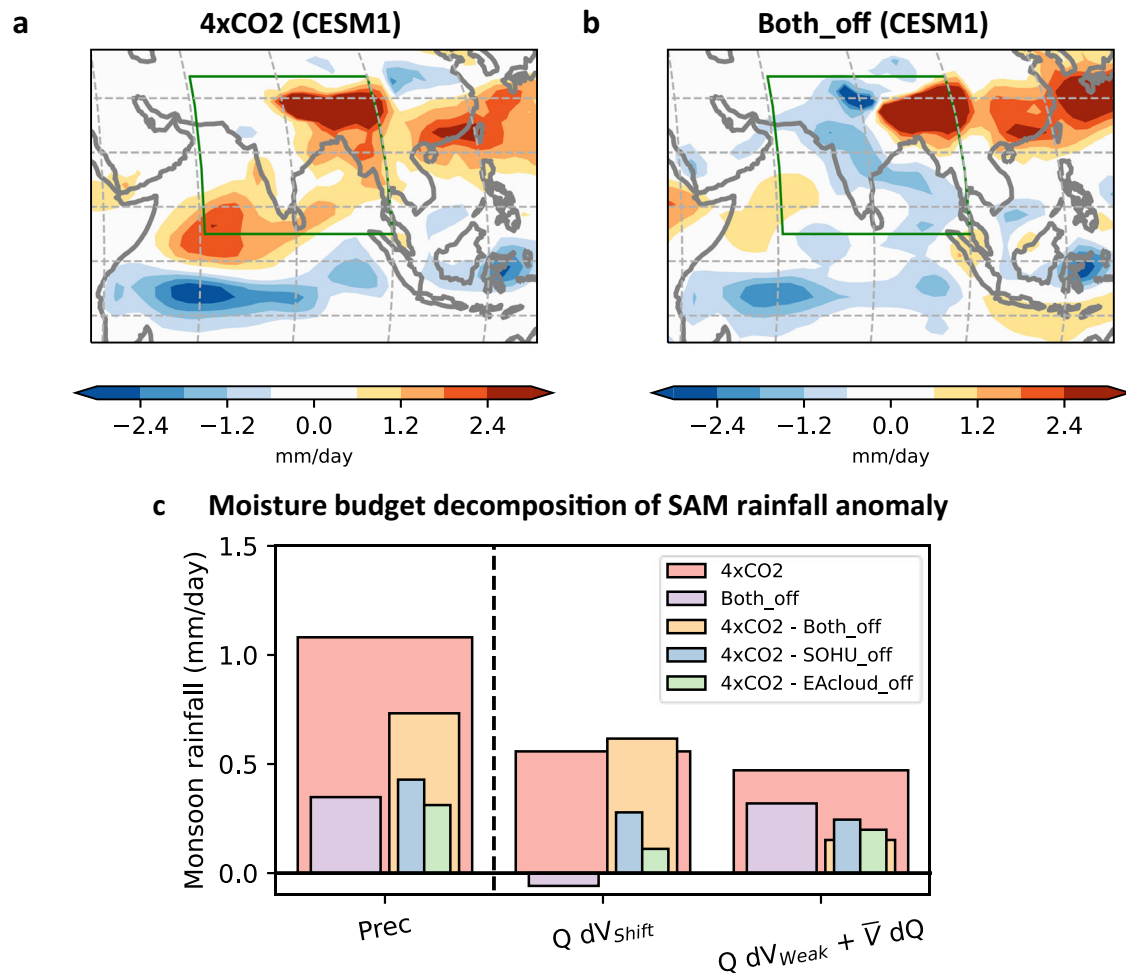


Fig. 4 | Changes of SAM rainfall in the CESM partially-coupled simulations. **a, b** CESM1 JJA-mean precipitation anomalies of abrupt-4xCO2 experiment (years 21–30). **a** Standard 4xCO2 experiment, **b** 4xCO2 experiment without Eurasia

extra-tropical cloud feedback and SO heat uptake (**Both_off**), and **(c)** Anomalous monsoon rainfall and moisture budget decomposition (the decomposition is identical to that in Fig. 1c). The thinner bars indicate the decomposition of the wider bars.

where the overbar indicates the JJA climatology in the baseline climate, and $d(\cdot)$ indicates the anomalies. \mathbf{V} and Q represent the horizontal wind field and the specific humidity field, respectively. Equation (4) represents the conventional moisture budget: the precipitation changes (dP) can be attributed to the changes in evaporation (dE), as well as the changes in moisture flux convergence associated with mean-flow advection (the second term on the right-hand side). The three terms in the integration on the right-hand side represent the contributions from anomalous moisture content, anomalous circulation, and the non-linear interaction between them. The residual term accounts for the contributions from transient eddy, and the numerical error arising from interpolation processes.

A modified moisture budget is proposed by isolating the weakening and shift components of dV :

$$dV = dV_{weak} + dV_{shift} \tag{5}$$

Substituting dV in Eq. (4) yields

$$dP = dE - \frac{1}{\rho g} \int_0^{ps} \left[\nabla \cdot (\bar{V}dQ) + \nabla \cdot (QdV_{shift}) + \nabla \cdot (QdV_{weak}) \right] dp + residual. \tag{6}$$

The second and third terms within the integration on the right-hand side account for the contributions associated with the shift and weakening of circulation, respectively.

Calculation of energy flux potential and regional EFE

Following Boos and Korty³⁴, the energy flux potential χ is defined as the inverse Laplacian of column-integrated MSE divergence:

$$\nabla^2 \chi = \nabla \cdot \int_0^{ps} \mathbf{v}h \frac{dp}{g} \sim NEI, \tag{7}$$

where \mathbf{v} indicates the horizontal wind, h the MSE, ps the surface pressure, g the gravitational acceleration, and ∇^2 the Laplacian operator. As the heat content changes of the atmosphere are usually negligible for a long-term climatology, the column-integrated MSE divergence is approximated by NEI in the calculation. To obtain a unique solution when calculating the inverse Laplacian, the global-mean value of energy flux potential is subtracted.

By definition, the gradient of energy flux potential represents the divergent (irrotational) component of atmospheric energy transport, noting as (uh, vh) here. To compute the regional EFE in the Indian Ocean sector, we first take the zonal average of energy flux potential between 60°E-100°E; the EFE is then defined as the latitude where $vh = 0$ and $\frac{dvh}{dy} > 0$.

Implied energy transport in 2D map

The anomalous energy flux potential can be expressed as

$$\nabla^2 d\chi = dNEI, \tag{8}$$

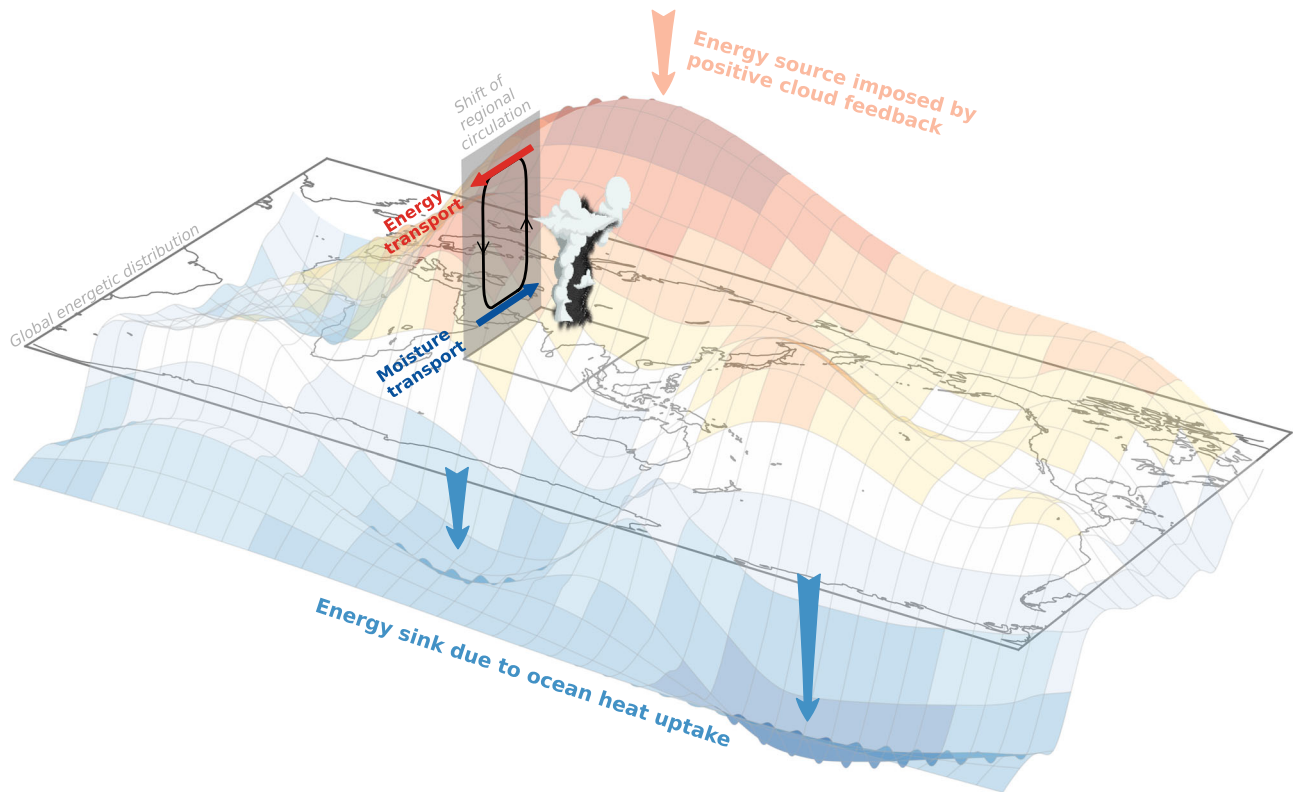


Fig. 5 | A schematic diagram showing the shift of deep convections toward the SAM region under warming. The shading represents the energy flux potential anomalies, with reds corresponding to negative anomalies (anomalous energy source) and blues corresponding to positive anomalies (anomalous energy sink); the z-axis of the energy flux potential anomalies is reversed for visualization purpose.

The light red and light blue arrows mark the extra-tropical energy sources and sinks. The vertical cross-section shows the regional circulation responses over the South Asia longitudinal sector; the dark red and blue arrows illustrate the meridional transport of energy and moisture over this sector.

As the Laplacian operator is linear, and so does its inverse, the anomalous energy flux potential caused by global NEI anomalies may be expressed as a summation of the contributions of anomalous NEI from different regions:

$$d\chi = \sum_i d\chi_{reg(i)}, \tag{9}$$

$$\nabla^2 d\chi_{reg(i)} = dNEI_{reg(i)}, \tag{10}$$

where *reg* indicates an arbitrary set of regions those summed up to covers all over the globe. For each subregion *reg(i)*, the contribution of anomalous NEI within this region to the anomalous energy flux potential is evaluated by the inverse Laplacian of *dNEI_{reg(i)}*, which equals *dNEI* within the subregion *reg(i)* and is zero elsewhere. Ideally, *dχ_{reg(i)}* can be thought of as the anomalous energy flux potential in response to the anomalous NEI within the region *reg(i)*, assuming that the energy transport is extremely efficient in redistributing energy globally. The contribution of regional NEI anomalies, *dNEI_{reg(i)}*, to the regional EFE shift in the Indian Ocean sector is then estimated by adding the associated energy flux potential anomalies, *dχ_{reg(i)}*, to the climatology energy flux potential in baseline climate ($\bar{\chi}$); the corresponding Indian Ocean EFE location of $\bar{\chi} + d\chi_{reg(i)}$ is calculated and then compared to the EFE location in the baseline climate.

As the anomalous NEI equals the summation of changes in cloud radiative effects, changes in clear-sky TOA fluxes, and changes in surface fluxes, we may further evaluate the contributions of regional cloud feedback and ocean heat uptake to *dχ_{reg(i)}*, following similar definition in Eq. (10):

$$\nabla^2 d\chi_{reg(i)-CRE} = dCRE_{reg(i)}, \tag{11}$$

$$\nabla^2 d\chi_{reg(i)-OHU} = dOHU_{reg(i)}, \tag{12}$$

where *SUR* represents surface fluxes, and *CRE* represents cloud radiative effects at TOA. The *CRE* is adjusted by radiative kernel⁵⁷ to remove the masking effects of clouds on the changes in surface albedo, water vapor, and temperature.

CESM1 simulations

A fully-coupled climate model, CESM1, is used in this study. A 50-year-long piControl simulation (**PI**) is conducted, as well as several 30-year-long abrupt-4xCO2 simulations: a standard abrupt-4xCO2 simulation (**4xCO2**), and three partially-coupled abrupt-4xCO2 simulations with suppressed Eurasia Continent cloud feedback (**EAcldoff**) or suppressed impacts of Southern Ocean heat uptake (**SOHUoff**), or with both the processes suppressed (**Bothoff**). These abrupt-4xCO2 experiments are identical except the suppression of regional cloud feedback or ocean processes, as will be described later. Each experiment contains three ensembles. The anomalies are obtained by subtracting the 50-years climatology of **PI** simulation from the average over years 21–30 in the abrupt-4xCO2 simulations.

Regional cloud-locking method

To suppress the cloud feedback over the Eurasia Continent in the **EAcldoff** and **Bothoff** simulations, a cloud-locking method⁵⁸ is applied. In the **PI** simulation, the cloud properties that are necessary for the calculation of radiation (include liquid and ice cloud fraction, in-cloud liquid/ice/snow water path, effective diameter for ice and snow, and size distribution parameters of liquid drops) are saved at every radiative time

step (every 2 h). These cloud properties are then read by the **EAcldoff** and **Both_off** simulations: over the mid-latitudes of the Eurasia Continent (0–140° E, 40–70° N), the cloud properties in the **PI** simulation are used in the calculations of radiative fluxes, so that the cloud radiative effects are decoupled from the current background environment in the model; in other regions, the cloud radiative effects are interactive with the background environment.

Southern Ocean pacemaker simulations

The impacts of ocean heat uptake over the Southern Ocean are minimized by nudging the SST over the Southern Ocean toward a “non-heat uptake” SST pattern. First, we estimate the warming rate of Southern Ocean in the absence of heat uptake by the outputs of the CESM1 slab ocean experiments provided by Hu et al.⁵⁹ (Supplementary Fig. 8b). In their experiments, the climatological ocean heat transport divergence in a pre-industrial simulation with dynamical ocean is prescribed as the “Q-flux” into the slab ocean model. Two slab ocean experiments, a control simulation and a doubled-CO₂ simulation, are then conducted. The slab ocean experiments are integrated for 60 years, and the last 50 years are used to calculate the equilibrium responses. As the Q-flux are identical in the two experiments, the differences between the two simulations represents the impacts of warming without changes in ocean heat uptake.

Next, the SST anomalies in the slab ocean models (dTS_{SOM}) are added to the daily SST outputs of the last 30 years in our **PI** simulation (TS_{PI}) to generate a 30-year-long daily SST data:

$$TS_{prescribe} = TS_{PI} + \frac{d\widetilde{TS}_{4xCO_2}}{d\widetilde{TS}_{SOM}} dTS_{SOM}, \quad (13)$$

where dTS_{4xCO_2} represents the SST anomalies in our **4xCO₂** simulation, and $\widetilde{(\)}$ indicates tropical mean and annual mean. The factor $d\widetilde{TS}_{4xCO_2}/d\widetilde{TS}_{SOM}$ is a normalization factor which rescales the SST anomaly in slab ocean model, so that the warming rate in $TS_{prescribe}$ can be in line with that in the **4xCO₂** simulation. In this way, $TS_{prescribe}$ preserves the pace of warming in the **4xCO₂** simulation, while the warming pattern is identical to that in the slab ocean model without anomalous ocean heat uptake.

As a final step, in the **SOHU_off** and **Both_off** simulations, the SST over the Southern Ocean (30–70° S) is nudged toward $TS_{prescribe}$, while it is free to evolve elsewhere. This is done by adding a relaxation term in the top-most layer of ocean model:

$$\frac{dT}{dt} = Adv + Dif + Sur + \frac{TS_{prescribe} - T}{\tau}. \quad (14)$$

Where the left-hand side represents the temperature tendency; *Adv*, *Dif*, and *Sur* represent the tendency associated with advection, diffusion, and surface fluxes, respectively, in the top layer. The last term on the right-hand side represents the relaxation toward $TS_{prescribe}$ with a relaxation timescale of $\tau=1$ h. By doing so, the SST in these simulations are unaffected by the ocean heat uptake over the Southern Ocean.

Data availability

The CMIP6 data can be downloaded via <https://esgf-node.llnl.gov/projects/cmip6/>. The outputs of the partially-coupled CESM1 simulations used in this study can be downloaded via zenodo.org, (<https://doi.org/10.5281/zenodo.10906259>).

Code availability

The codes to produce the analyses presented in this study are available upon request from the corresponding author.

Received: 20 June 2024; Accepted: 12 November 2024;

Published online: 21 December 2024

References

- Douglas, I. Climate change, flooding and food security in south Asia. *Food Secur.* **1**, 127–136 (2009).
- Christensen, J. H. et al. Climate phenomena and their relevance for future regional climate change. *Intergov. Panel Clim. Chang.* **9781107057**, 1217–1308 (2013).
- Xie, S. P. et al. Towards predictive understanding of regional climate change. *Nat. Clim. Chang.* **5**, 921–930 (2015).
- Endo, H. & Kitoh, A. Thermodynamic and dynamic effects on regional monsoon rainfall changes in a warmer climate. *Geophys. Res. Lett.* **41**, 1704–1710 (2014).
- Zhu, Y. Variations of the summer Somali and Australia cross-equatorial flows and the implications for the Asian summer monsoon. *Adv. Atmos. Sci.* **29**, 509–518 (2012).
- Latif, M. et al. Reconstructing, Monitoring, and Predicting Multidecadal-Scale Changes in the North Atlantic Thermohaline Circulation with Sea Surface Temperature. *J. Clim.* **17**, 1605–1614 (2004).
- Sandeep, S. & Ajayamohan, R. S. Poleward shift in Indian summer monsoon low level jetstream under global warming. *Clim. Dyn.* **45**, 337–351 (2015).
- Zhou, T., Yu, R., Li, H. & Wang, B. Ocean forcing to changes in global monsoon precipitation over the recent half-century. *J. Clim.* **21**, 3833–3852 (2008).
- Ganguly, D., Rasch, P. J., Wang, H. & Yoon, J. H. Climate response of the South Asian monsoon system to anthropogenic aerosols. *J. Geophys. Res. Atmos.* **117**, 1–20 (2012).
- Polson, D., Bollasina, M., Hegerl, G. C. & Wilcox, L. J. Decreased monsoon precipitation in the Northern Hemisphere due to anthropogenic aerosols. *Geophys. Res. Lett.* **41**, 6023–6029 (2014).
- Jiang, Y., Li, J., Wang, B., Yang, Y. & Zhu, Z. Weakening of decadal variation of Northern Hemisphere land monsoon rainfall under global warming. *npj Clim. Atmos. Sci.* **6**, 1–9 (2023).
- Seager, R., Naik, N. & Vecchi, G. A. Thermodynamic and dynamic mechanisms for large-scale changes in the hydrological cycle in response to global warming. *J. Clim.* **23**, 4651–4668 (2010).
- Turner, A. G. & Annamalai, H. Climate change and the South Asian summer monsoon. *Nat. Clim. Chang.* **2**, 587–595 (2012).
- Li, Z., Sun, Y., Li, T., Chen, W. & Ding, Y. Projections of south Asian summer monsoon under global warming from 1.5° to 5°C. *J. Clim.* **34**, 7913–7926 (2021).
- Held, I. M. & Soden, B. J. Robust responses of the hydrological cycle to global warming. *J. Clim.* **19**, 5686–5699 (2006).
- Lee, D. et al. Impacts of half a degree additional warming on the Asian summer monsoon rainfall characteristics. *Environ. Res. Lett.* **13**, 044033 (2018).
- Cherchi, A., Alessandri, A., Masina, S. & Navarra, A. Effects of increased CO₂ levels on monsoons. *Clim. Dyn.* **37**, 83–101 (2011).
- Li, X., Ting, M., Li, C. & Henderson, N. Mechanisms of Asian Summer Monsoon Changes in Response to Anthropogenic Forcing in CMIP5 Models*. *J. Clim.* **28**, 4107–4125 (2015).
- Jiang, Y., Zhu, Z., Li, J., Miao, L. & Miao, Z. Changes of mean and extreme precipitation and their relationship in Northern Hemisphere land monsoon domain under global warming. *Int. J. Climatol.* **43**, 5536–5552 (2023).
- Roxy, M. K. et al. Drying of Indian subcontinent by rapid Indian ocean warming and a weakening land-sea thermal gradient. *Nat. Commun.* **6**, 7423 (2015).
- Krishnan, R. et al. Will the South Asian monsoon overturning circulation stabilize any further? *Clim. Dyn.* **40**, 187–211 (2013).
- Sandeep, S., Ajayamohan, R. S., Boos, W. R., Sabin, T. P. & Praveen, V. Decline and poleward shift in Indian summer monsoon synoptic activity in a warming climate. *Proc. Natl Acad. Sci. USA* **115**, 2681–2686 (2018).
- Kjellsson, J. Weakening of the global atmospheric circulation with global warming. *Clim. Dyn.* **45**, 975–988 (2015).

24. Sooraj, K. P., Terray, P. & Mujumdar, M. Global warming and the weakening of the Asian summer monsoon circulation: assessments from the CMIP5 models. *Clim. Dyn.* **45**, 233–252 (2015).
25. Biasutti, M. et al. Global energetics and local physics as drivers of past, present and future monsoons. *Nat. Geosci.* **11**, 392–400 (2018).
26. Geen, R., Bordoni, S., Battisti, D. S. & Hui, K. Monsoons, ITCZs, and the Concept of the Global Monsoon. *Rev. Geophys.* **58**, 1–45 (2020).
27. Kang, S. M., Held, I. M., Frierson, D. M. W. & Zhao, M. The response of the ITCZ to extratropical thermal forcing: Idealized slab-ocean experiments with a GCM. *J. Clim.* **21**, 3521–3532 (2008).
28. Schneider, T., Bischoff, T. & Haug, G. H. Migrations and dynamics of the intertropical convergence zone. *Nature* **513**, 45–53 (2014).
29. Donohoe, A., Marshall, J., Ferreira, D. & Mcgee, D. The relationship between ITCZ location and cross-equatorial atmospheric heat transport: From the seasonal cycle to the last glacial maximum. *J. Clim.* **26**, 3597–3618 (2013).
30. Bischoff, T. & Schneider, T. The equatorial energy balance, ITCZ position, and double-ITCZ bifurcations. *J. Clim.* **29**, 2997–3013 (2016).
31. Adam, O., Bischoff, T. & Schneider, T. Seasonal and interannual variations of the energy flux equator and ITCZ. Part II: Zonally varying shifts of the ITCZ. *J. Clim.* **29**, 7281–7293 (2016).
32. Keshtgar, B., Alizadeh-Chooabari, O. & Irannejad, P. Seasonal and interannual variations of the intertropical convergence zone over the Indian Ocean based on an energetic perspective. *Clim. Dyn.* **54**, 3627–3639 (2020).
33. Lu, J. et al. The Leading Modes of Asian Summer Monsoon Variability as Pulses of Atmospheric Energy Flow. *Geophys. Res. Lett.* **48**, e2020GL091629 (2021).
34. Boos, W. R. & Korty, R. L. Regional energy budget control of the intertropical convergence zone and application to mid-Holocene rainfall. *Nat. Geosci.* **9**, 892–897 (2016).
35. Chou, C. & Chen, C. A. Depth of convection and the weakening of tropical circulation in Global Warming. *J. Clim.* **23**, 3019–3030 (2010).
36. Jeevanjee, N. Three Rules for the Decrease of Tropical Convection With Global Warming. *J. Adv. Model. Earth Syst.* **14**, e2022MS003285 (2022).
37. Ma, J. et al. Responses of the Tropical Atmospheric Circulation to Climate Change and Connection to the Hydrological Cycle. *Annu. Rev. Earth Planet. Sci.* **46**, 549–580 (2018).
38. Vecchi, G. A. & Soden, B. J. Global warming and the weakening of the tropical circulation. *J. Clim.* **20**, 4316–4340 (2007).
39. Ma, J., Xie, S. P. & Kosaka, Y. Mechanisms for tropical tropospheric circulation change in response to global warming. *J. Clim.* **25**, 2979–2994 (2012).
40. Kang, S. M., Frierson, D. M. W. & Held, I. M. The Tropical Response to Extratropical Thermal Forcing in an Idealized GCM: The Importance of Radiative Feedbacks and Convective Parameterization. *J. Atmos. Sci.* **66**, 2812–2827 (2009).
41. Ramesh, N. & Boos, W. R. The Unexpected Oceanic Peak in Energy Input to the Atmosphere and Its Consequences for Monsoon Rainfall. *Geophys. Res. Lett.* **49**, e2022GL099283 (2022).
42. Mamalakis, A. et al. Zonally contrasting shifts of the tropical rain belt in response to climate change. *Nat. Clim. Chang.* **11**, 143–151 (2021).
43. Pearce, F. A. & Bodas-Salcedo, A. Implied Heat Transport from CERES Data: Direct Radiative Effect of Clouds on Regional Patterns and Hemispheric Symmetry. *J. Clim.* **36**, 4019–4030 (2023).
44. Zhou, W., Leung, L. R. & Lu, J. The Role of Interactive Soil Moisture in Land Drying Under Anthropogenic Warming. *Geophys. Res. Lett.* **50**, e2023GL105308 (2023).
45. Armour, K. C., Marshall, J., Scott, J. R., Donohoe, A. & Newsom, E. R. Southern Ocean warming delayed by circumpolar upwelling and equatorward transport. *Nat. Geosci.* **9**, 549–554 (2016).
46. Li, Q., Luo, Y., Lu, J. & Liu, F. The Role of Ocean Circulation in Southern Ocean Heat Uptake, Transport, and Storage Response to Quadrupled CO₂. *J. Clim.* **35**, 3565–3582 (2022).
47. Liu, W., Lu, J., Xie, S. P. & Fedorov, A. Southern Ocean Heat Uptake, redistribution, and storage in a warming climate: The role of meridional overturning circulation. *J. Clim.* **31**, 4727–4743 (2018).
48. Morrison, A. K., Griffies, S. M., Winton, M., Anderson, W. G. & Sarmiento, J. L. Mechanisms of Southern Ocean heat uptake and transport in a global eddying climate model. *J. Clim.* **29**, 2059–2075 (2016).
49. Freychet, N., Hsu, H. H., Chou, C. & Wu, C. H. Asian summer monsoon in CMIP5 projections: A link between the change in extreme precipitation and monsoon dynamics. *J. Clim.* **28**, 1477–1493 (2015).
50. Hu, Z. Z., Latif, M., Roeckner, E. & Bengtsson, L. Intensified Asian summer monsoon and its variability in a coupled model forced by increasing greenhouse gas concentrations. *Geophys. Res. Lett.* **27**, 2681–2684 (2000).
51. Lau, W. K. M. & Kim, K. M. Competing influences of greenhouse warming and aerosols on Asian summer monsoon circulation and rainfall. *Asia Pac. J. Atmos. Sci.* **53**, 181–194 (2017).
52. Li, R., Lv, S., Han, B., Gao, Y. & Meng, X. Projections of South Asian summer monsoon precipitation based on 12 CMIP5 models. *Int. J. Climatol.* **37**, 94–108 (2017).
53. Menon, A., Levermann, A., Schewe, J., Lehmann, J. & Frieler, K. Consistent increase in Indian monsoon rainfall and its variability across CMIP-5 models. *Earth Syst. Dyn.* **4**, 287–300 (2013).
54. Wang, B., Jin, C. & Liu, J. Understanding Future Change of Global Monsoons Projected by CMIP6 Models. *J. Clim.* **33**, 6471–6489 (2020).
55. Sherwood, S. C. et al. An Assessment of Earth's Climate Sensitivity Using Multiple Lines of Evidence. *Rev. Geophys.* **58**, 1–93 (2020).
56. Singh, D., Ghosh, S., Roxy, M. K. & McDermid, S. Indian summer monsoon: Extreme events, historical changes, and role of anthropogenic forcings. *WIREs Clim. Chang.* **10**, e571 (2019).
57. Pendergrass, A. G., Conley, A. & Vitt, F. Surface and top-of-atmosphere radiative feedback kernels for CESM-CAM5. *Earth Syst. Sci. Data Discuss.* **5**, 1–14 (2017).
58. Ceppi, P. & Hartmann, D. L. Clouds and the Atmospheric Circulation Response to Warming. *J. Clim.* **29**, 783–799 (2016).
59. Hu, S., Xie, S. P. & Kang, S. M. Global Warming Pattern Formation: The Role of Ocean Heat Uptake. *J. Clim.* **35**, 1885–1899 (2022).

Acknowledgements

Y.-J. Chen and Y.-T. Hwang were supported by Ministry of Science and Technology of Taiwan (NSTC 112-2111-M-002-016-MY4). J. Lu was supported by Office of Science, U.S. Department of Energy Biological and Environmental Research as part of the Regional and Global Model Analysis program area.

Author contributions

Y.-J.C. and Y.-T.H. designed and performed research; Y.-J.C. analyzed data; J.L. provided important insights for interpreting the results; Y.-J.C., Y.-T.H., and J.L. wrote the paper.

Competing interests

The authors declare no competing interests.

Additional information

Supplementary information The online version contains supplementary material available at <https://doi.org/10.1038/s41612-024-00843-7>.

Correspondence and requests for materials should be addressed to Yen-Ting Hwang.

Reprints and permissions information is available at <http://www.nature.com/reprints>

Publisher's note Springer Nature remains neutral with regard to jurisdictional claims in published maps and institutional affiliations.

Open Access This article is licensed under a Creative Commons Attribution-NonCommercial-NoDerivatives 4.0 International License, which permits any non-commercial use, sharing, distribution and reproduction in any medium or format, as long as you give appropriate credit to the original author(s) and the source, provide a link to the Creative Commons licence, and indicate if you modified the licensed material. You do not have permission under this licence to share adapted material derived from this article or parts of it. The images or other third party material in this article are included in the article's Creative Commons licence, unless indicated otherwise in a credit line to the material. If material is not included in the article's Creative Commons licence and your intended use is not permitted by statutory regulation or exceeds the permitted use, you will need to obtain permission directly from the copyright holder. To view a copy of this licence, visit <http://creativecommons.org/licenses/by-nc-nd/4.0/>.

© The Author(s) 2024